Third Joint Eurohaptics Conference and Symposium on Haptic Interfaces
for Virtual Environment and Teleoperator Systems
Salt Lake City, UT, USA, March 18-20, 2009

Effects of Haptic Device Attributes on Vibration Detection Thresholds

Curt Salisbury*
BioRobotics Laboratory
Stanford University, USA

R. Brent Gillespie†
The Haptix Laboratory
University of Michigan, USA

Hong Tan‡
Haptic Interface Research Laboratory
Purdue University, USA

Federico Barbagli§
BioRobotics Laboratory
Stanford University, USA

J. Kenneth Salisbury¶
BioRobotics Laboratory
Stanford University, USA

Abstract

Human vibrotactile detection experiments were used to compare temporal sinusoids displayed on three commercial haptic devices to a high-fidelity linear voice-coil actuator. The three commercial haptic devices we used span the cost spectrum, supposing that cost of a device is correlated with the fidelity of its virtual textures. This turned out not to be the case. The results indicated that none of the three haptic devices we tested were able to render perceptually distortion-free, periodically regular vibrations at detection threshold levels. Further investigation into the electrical and mechanical device properties that limited the performance of these devices revealed that D/A resolution, amplifier non-linearity and stiction were the primary sources of signal corruption.

Index Terms: H.5.2 [Information Interfaces and Presentation]: User Interfaces—Haptic I/O

1 Introduction

Recent advances in haptics technology have produced a plethora of haptic force feedback devices that span a wide range of electrical and mechanical properties as well as price. How does one compare one device with another? More importantly, how should one choose a haptic device with the best performance / price ratio for a given application? Similar questions are asked when one is faced with the task of choosing the best video projector or the best audio amplifier. In the case of video projectors, the contrast sensitivity function was found to be a good indicator of performance[1], and we are all familiar with the spectral transfer function for audio amplifiers. This led us to investigate the haptic equivalent of a frequency-based performance evaluation of force-feedback devices. Specifically, we sought to measure the human detection thresholds of vibrations. To the extent that thresholds are found to vary across devices with different electrical and mechanical specifications, we would then investigate the primary sources for the observed discrepancies in thresholds.

Transmitted vibrations have been effectively used as a way to render virtual textures through point-contact force-feedback haptic devices. One might argue that a "good" haptic device is one that can render "realistic-feeling" textures. Realism, however, is itself a matter of perception. From a signal flow point of view, the virtual textures are first defined mathematically in the rendering algorithm. Forces are then output through the haptic device to present the texture to a human user. The haptic devices inevitably filter out some of the intended signals and may also add some noise to the output forces. Once the proximal stimuli reach the skin, they excite mechanoreceptors. The nerve fibers connected to the mechanoreceptors fire action potentials which travel through afferent neurons to the brain where the neurophysiological signals are interpreted and a percept is formed. In order for a virtual texture to feel real it needs to present only the proximal stimuli that matter to forming the intended sensations. The absence of these stimuli or the presence of unintended stimuli that pass through these mechanisms will compromise the sense of realism of a texture. In contrast, the presence of any other stimuli that are subsequently filtered out by these neural and cognitive mechanisms will not compromise the sense of realism of a texture.

The extensive database of physiological and psychophysical information found in the literature helps us understand which of the proximal stimuli presented actually have a significant influence on how textures are perceived. Some have generated mathematical models of this filtering behavior[2] in an effort to predict how an arbitrary proximal stimulus will be perceived. Because these mechanisms are well understood and fairly consistent across participants, human perception can be used to objectively evaluate the realism of virtual textures and, more specifically, the ability of haptic hardware to render realistic virtual textures.

Few have investigated the effect of haptic system attributes on the tactile perceptual realism of virtual textures. To our knowledge, Choi and Tan are the only ones to have begun to address this issue. They investigated the effects of virtual stiffness values[3], rendering algorithm[4], and sample rate[5] on the existence of realism-compromising instability. They found that low sample rates, large stiffnesses, and a poor selection of rendering algorithm introduced unintended percepts. They formulated guidelines for the limits of sample rates, stiffnesses, and rendering algorithms that would prevent the existence of the unintended percepts. Campion and Hayward investigated the effect of electrical and mechanical characteristics of the haptic device on the proximal stimuli[6], but perception was not used to qualify these effects. We wish to extend the work of these researchers by using human perception to measure the effect of electrical and mechanical attributes of a haptic device on the perceived realism of haptic textures.

The human-device interface for the haptic devices we work with are rigid probes. When participants explore textures via a rigid probe, the texture has been shown to be encoded temporally through transmitted vibrations[7] through four types of mechanoreceptors, depending on the spectral range of the vibrotactile signal[8]. In the absence of masking stimuli, however, detection threshold levels are primarily governed by two channels. The psychophysical P channel determines detection thresholds for vibrotactile stimuli between 40 Hz and 800 Hz and is correlated with the fast acting (FA) II afferent fibers whose nerve endings are the Pacinian Corpuscles[9]. The NP I channel determines detection thresholds between 10 Hz and 40 Hz and is correlated with the FA I fibers whose nerve endings are believed to be the Meissner corpuscles.

Because a texture perceived through a rigid probe is coded tem-

*e-mail: curtsu@stanford.edu
†e-mail:brentg@umich.edu
‡e-mail:hongtan@purdue.edu
§e-mail:fed_barbagli@hansenmedical.com
¶e-mail:jks@robotics.stanford.edu

porally, initial insight into the ability of a haptic device to render texture can be gained by using temporal (vibrotactile) stimuli rather than spatial stimuli. Consequently, this study will focus exclusively on the effects of electrical and mechanical characteristics on the perception of temporal sinusoidal vibrations. We will essentially simulate the vibrations resulting from moving a sinusoidal grating under a stationary rigid tool. This abstraction will enable us to control for texture rendering algorithms, encoder resolution, and closed loop behavior and simplify the quantitative analysis of the effects of the remaining device attributes, without the possible confounding effects of hand movements.

Pyschophysical studies fall into one of three categories: detection, discrimination, or identification. In our judgment, detection experiments are likely to be the most taxing of the three types of perceptual experiments on a haptic device. This is due to the need to render vibrations at minute amplitudes that challenge both the position encoder resolution as well as the force output resolution. We reasoned that the presence of electrical and/or mechanical noises would mask the weak vibrational signals and therefore raise the human detection thresholds. In addition, the presence of noises above human detection thresholds will qualitatively affect the perceived quality of virtual textures (see, for example, Fig. 9 in [3]). We therefore expect detection experiments to reveal the most about what limits a haptic device from rendering realistic textures. Consequently, the psychophysical experiments we use to measure device performance are displacement detection experiments using vibrotactile stimuli.

The first objective of this paper is to evaluate the ability of three commercially available haptic devices to render temporal sinusoids as measured by a psychophysical displacement detection experiment. Results are compared to the ability of a high-bandwidth linear voice-coil actuator to render temporal sinusoids. Necessary criteria used to determine if a haptic device has the ability to render realistic textures are: (1) the estimated detection thresholds identified are similar to that of the voice-coil for each tested vibratory frequency, (2) there is no perceptible harmonic distortion, and (3) the proximal stimuli are consistent and periodic in nature for a given commanded signal. To the extent that phsychophysical and temporal results do not meet all of these criteria, the device is deemed to be deficient in its ability to render realistic textures.

The second objective of this paper is to investigate the electrical and mechanical design attributes, and their values, of those devices that are deficient in their ability to render realistic textures. Specifically, we investigate those attributes that prevent the devices from rendering clean vibrations. We will show that the attributes that will have the most detrimental effect on the ability of these haptic devices to render realistic virtual textures are those that exhibit nonlinear behavior. Among these are backdrive static friction, actuator signal quantization, and amplifier hysteresis.

2 Methods

2.1 Apparatus

The three commercially available haptic devices used in our study were intended to span the cost spectrum, supposing that cost of a device is correlated with the fidelity of its virtual textures. These haptic interfaces are the PHANTOM Premium 1.0 (Sensable Technologies, Woburn, MA), the PHANTOM Omni (Sensable Technologies, Woburn, MA), and the Falcon (Novint, Albuquerque, NM). Approximate cost for each device is $20,000, $2,000, and $200 respectively. A picture of these devices, along with the linear voice coil actuator is shown in Fig. 1. Each device, with the exception of the voice coil, was controlled through CHAI3d[10], a freeware platform designed for use with a variety of haptic devices.

The voice coil we use is from an old disk drive head actuator mechanism. The voice coil uses coreless aluminum windings attached to an aluminum flange for tool attachment, all mounted on

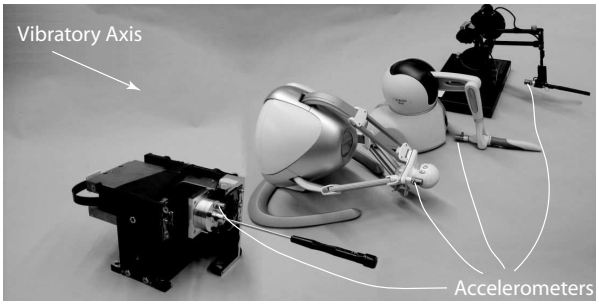

Figure 1: Linear voice-coil actuator and haptic devices for detection experiment. Arrows illustrate the axis of vibrotactile stimulation.

precision linear bearings. The mechanical dynamics of this system are well described by a simple mass, 210 grams in this case. Consequently, the transfer function relating winding current to acceleration has a wide and flat bandwidth, extending beyond 1 kHz. The electrical inductance and resistance are 1.02 mH and 8.4 Ω, respectively. Consequently the transfer function relating drive current to drive voltage is flat up to approximately 1.3 kHz. When cascaded, these transfer functions reveal a scalar relationship between drive voltage and acceleration of the unloaded voice coil for frequencies up to approximately 1 kHz. We drive this device directly through the 16 bit digital-to-analog (D/A) converter of a National Instruments data acquisition board (National Instruments PCI-6259, Austin, TX) by commanding a reference voltage. The D/A of this board is capable of sourcing up to 5 mA. Because the currents required for our experiment are below this level, an additional inline current amplifier was unnecessary. The linear voice-coil actuator was used as a "gold standard", supposing that the superior electrical and mechanical behavior outlined above would generate detection thresholds limited only by human capability and not device attributes.

All devices are run on a PC operating Windows XP. All devices except for the voice coil are run at their servo loop rates of 1 kHz. The voice coil has a servo loop period of approximately 66.2 μs (a rate of $\approx$15 kHz) with a jitter (i.e. standard deviation calculated from 120,000 sampling periods) of approximately 9.2 μs. This large jitter is actually due to a few outliers of large periods.

Impedance type haptic devices operate by reading displacements (x_h) at the human-device interface, often a stylus, and calculating and converting force commands (f_c) to proximal stimuli in the form of forces (f_h). These forces consequently cause displacement variations on the skin of the hand holding the stylus. We use displacement x_h at the human-device interface to characterize the proximal stimulus. The haptic devices in our experimental pool use encoders to measure position, but we found that their resolution was insufficient to resolve the displacements for our purposes. Instead, we estimated displacements from an attached accelerometer. The accelerometer used (model 8702B25, Kistler Instrument Corp., Amherst, NY) measured 200 mV/g, ensuring good sensitivity of the accelerometer to low values of acceleration, and had a frequency range from 1 to 8000 Hz. An accelerometer mount was added to each of the four devices (see Fig. 1). The mounts were attached as close to the participant's hand as possible to ensure that it measured what the hand experienced. The mount and accelerometer weighed 2 grams and 8 grams respectively. The accelerometer was sampled through the 16-bit Analog-to-Digital port on the NI board at the same rate as the drive loop for the voice coil ($\approx$15 kHz).

2.2 Participants

Four males and one female (age 23-31 years old, average 26 years old) participated in the study. All were right handed by self report. All participants (P1-P5) had interacted with haptic devices prior to this experiment.

3 Procedure

The participant sat at a desk containing the haptic devices to be tested, a computer monitor, and a keyboard. They held the device interface with their dominant hand. For the spherical interface, they were instructed to hold it with a baseball-style grip. For the pen-like interfaces, they were told to hold the stylus like a pen. They were told to hold the pen parallel (or nearly parallel) to the axis of motion and still throughout the experiment. Fig. 1 shows the axis of motion used for each of the tested haptic devices. The participant's wrist and elbow were supported by foam pads to facilitate a natural posture and minimize fatigue. Participants wore headphones playing white noise to mask auditory cues coming from the haptic devices.

Two test frequencies ($f = 40, 160$ Hz) were used to compare thresholds of the four devices. The order of the frequencies and devices tested was randomized. In each trial, the participant was presented with a three-interval, forced-choice, one-up three-down adaptive method[11]. Because adapting around the proximal stimulus (x_h) is difficult, we instead chose to adapt around commanded force (f_c) amplitude. We expect this to be reasonable since we expect x_h to vary monotonically with f_c. While the voice coil was driven with a reference voltage, its linear relationship to commanded force was straightforward and so conversion from voltage to commanded force allowed the voice coil reference signal to be compared more directly to the commanded forces sent to the commercial haptic devices. Per this method, the participant was presented with three randomly ordered stimuli. Two of them were generated by a null reference signal ($f_c = 0, \forall t$) while the third was generated by the sinusoidal signal ($f_c = A_c \sin(2\pi f t)$). The participant used their non-dominant hand to communicate via the keyboard whether to cycle through to the next of the three stimuli or select the current stimulus as the one they identified to be unique from the other two. There was no limit to either the number of times they could cycle through the triplets or the time they could spend observing any individual stimulus. To prevent temporal edge effects, transitions between stimuli were modified by an exponential function with 1 s rise and fall times. The initial stimulus amplitude was set to be easily detectable by participants. Three consecutive correct responses resulted in a decrease in the amplitude of A_c. One incorrect response resulted in an increase of the amplitude of A_c. Modifications to the amplitude of A_c during the first 3 reversals were 4dB, and 1dB during the remaining 12 reversals, after which the test was over. Participants took a break between experiments on each device.

3.1 Analysis of position threshold

For each device and each frequency, the last twelve reversals (six A_c peaks and six A_c valleys) were used to calculate the detection thresholds ($\bar{A_c}$) and standard deviations (σ_A). Each peak-valley pair was averaged to generate a sample for the estimation of A_c. $\bar{A_c}$ is the mean of these six samples and σ_A is their standard deviation. Participants whose results did not converge were asked to repeat the experiment until convergence was obtained.

In order to determine displacement thresholds, the devices were run post-hoc at threshold level ($f_c = A_c \sin(2\pi f t)$) while the participant held the stylus and the accelerometer signal was recorded. A spectral analysis was conducted on the accelerometer signal to deduce the displacement threshold and signal purity while raw temporal data was used to determine signal regularity.

4 Results

We first present the commanded force detection thresholds ($\bar{A_c}$) in Fig. 2. The detectable commanded force sinusoid amplitudes sent to the Premium seem to be lower than those of the other two devices. The detectable amplitudes sent to the Falcon are the highest, followed by the Omni and the Voice coil. There was a bimodal distribution in the detectable amplitudes sent to the Phantom at 40 Hz. P2 and P3 detected thresholds of $\bar{A_c} \approx 10$ mN while P1, P4, and P5 detected thresholds at $\bar{A_c} \approx 1$ mN.

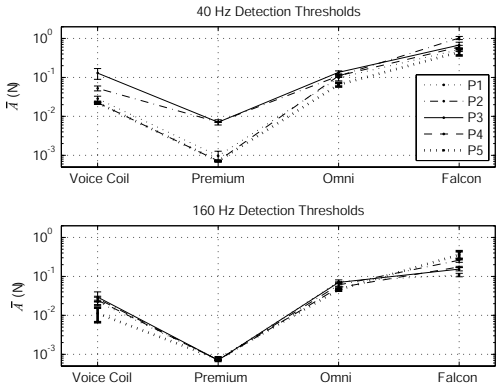

Figure 2: Commanded sinusoid detection thresholds for the three commercial haptic devices.

Fig. 3 contains the displacement spectra determined from the accelerometer measurements for P1. We compared these spectra to the detection thresholds identified by Israr et al[12]. These authors measured displacement detection thresholds of vibrations with a high-fidelity minishaker actuator. Because many more frequencies were tested in Israr et al, we use those data to get a sense for which spectral components from our experiments are likely suprathreshold and which are likely sub-threshold.

The spectra for P1 show that the voice coil produced the most distortion-free signal for both frequencies, which held true across all participants. Furthermore, though with some individual variation, the peaks appear to line up with the threshold data identified by Israr et al. These spectra for P1 show that all of the commercial haptic devices produced significant harmonic distortion for both frequencies, which also held true across all participants. Most notable is the signal presented by the Premium to P1. The magnitude of the 80 Hz component was closer to the detection threshold identified by Israr et al than the 40 Hz component and is the likely source of detection for that signal. This was also true for P4 and P5. While the data for P2 and P3 also exhibited significant distortion, only the 40 Hz signal was suprathreshold. With the Premium, some participants noticed a dramatic difference in the quality of the vibrations between clearly detectable signals and those at or near the threshold level. Spectral content at approximately 10 Hz is tremor induced by P1.

Inspection of the temporal data for the voice coil and Premium showed consistent periodicity with a fundamental frequency at the commanded frequency. The temporal data for the Omni and Falcon, however, showed aperiodic, sporadic responses, especially when driven by a 40 Hz signal. Fig. 4 shows a segment of the time response of the acceleration of the stylus of the Falcon held by P1 at threshold levels. There are 0.15 m/s^2 amplitude pulses between 1.05 s and 1.15 s but these decay to a 0.05 m/s^2 amplitude signal between 1.3 s and 1.4 s. The bursts of 0.15 m/s^2 pulses occur randomly. These data are also representative of those collected with the Omni.

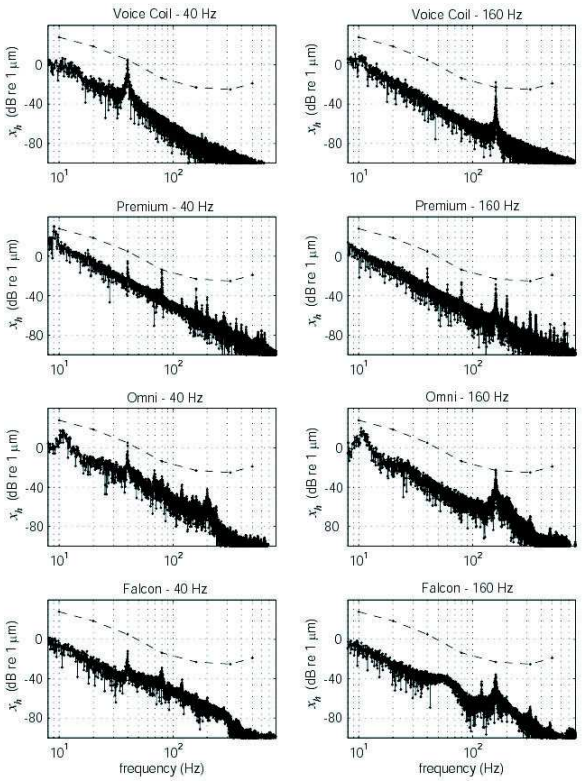

Figure 3: Displacement spectra for P1 for all devices and both frequencies. Dashed line segments connect threshold detection data collected by Israr et al.

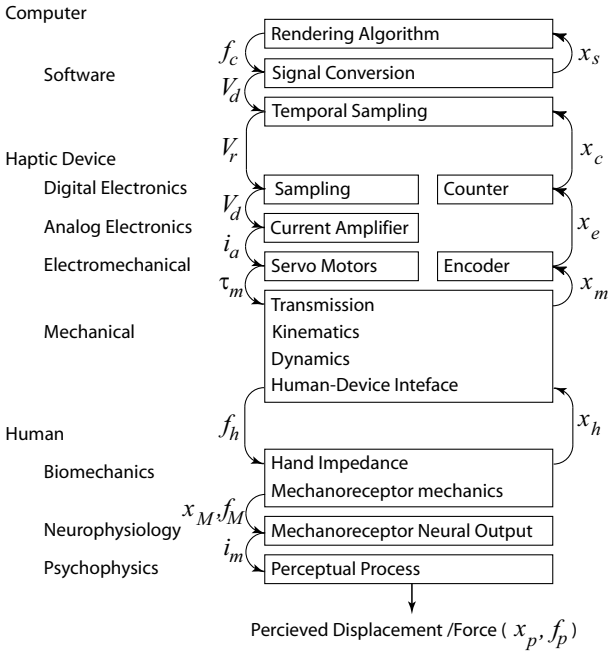

Figure 5: Block diagram of information flow from computer through haptic device to human and back.

5 Discussion

In contrast to the voice coil, none of the three commercially available haptic devices were capable of rendering perceptually distortion-free, periodically regular vibrations. Detection thresholds for the Premium were often dictated by harmonics rather than the fundamental frequency. The displacement behavior of the Falcon and Omni was sporadic in both the spectral content and associated amplitudes. Here we discuss the electrical and mechanical causes of these results.

To fully describe the electrical and mechanical behavior of a haptic device, there are a significant number of attributes that must be characterized. Hayward and Astley provide a comprehensive list of these attributes[13]. In Fig. 5 we represent the information flow through these electrical and mechanical modifiers that occurs during a haptic interaction.

It is apparent that the commanded force, f_c relates only in a distant sense to the perceived force, f_p, and the resultant displacement, x_p. The original f_c signal passes through many electrical and mechanical modifiers, each of which can mask desired signal features and introduce undesired features. The first modifier is the signal conversion which consists of the inverse kinematics and translation from joint torques to reference voltages (V_c). The next modifier is the servo loop of the haptic program which samples V_c in time and applies a zero order hold during the loop execution time. The output electronics then sample V_r in amplitude. Both sampling processes can introduce signal distortion. This signal (V_d) then passes through the current amplifier and this current (i_a) is converted to torque (τ_m) through a servo motor. The amplifier can introduce deadband and delay while the motor exhibits torque ripple. The torque passes through a transmission mechanism to the kinematic mechanism and terminates at the human-device interface with an applied force f_h and its associated resultant displacement x_h. All mechanical elements can exhibit backlash, stiction, viscous friction, elasticity, and have inertia. The perceived vibratory forces (f_p) and displacements (x_p) are the result of f_h and x_h being modified by physiological and psychophysical modifiers of the human. Because our experiments operated the haptic devices in open loop, we can ignore the feedback signals.

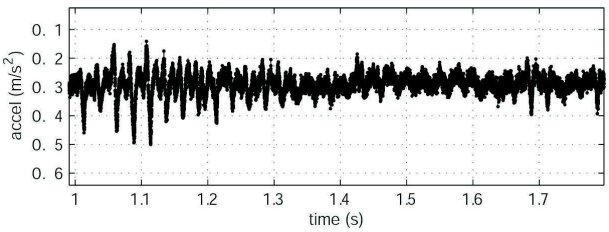

Figure 4: Temporal data sample from P1 on the Falcon

5.1 Digital electronics output resolution

Digital electronics output resolution was identified as a primary source of distortion in the Premium. This was made clear by observing V_d, a signal which is accessible on the Premium. Fig 6 shows the temporal and spectral data of V_d for 40 Hz threshold levels for P1 and P2, along with the temporal data of f_c and the spectral data of x_h. As is evident from the temporal data of V_d, the resolution of the digital-to-analog converter is 5 mV which corresponds to an f_c of 8 mN when the stylus is in the home position. The dashed horizontal lines in the plots of f_c show the transition values of the D/A. The D/A transition level closest to zero for our particular device is at f_c =-0.7 mN.

The commanded force threshold ($\bar{A_c}$)for P2 and P3 with the Pre-

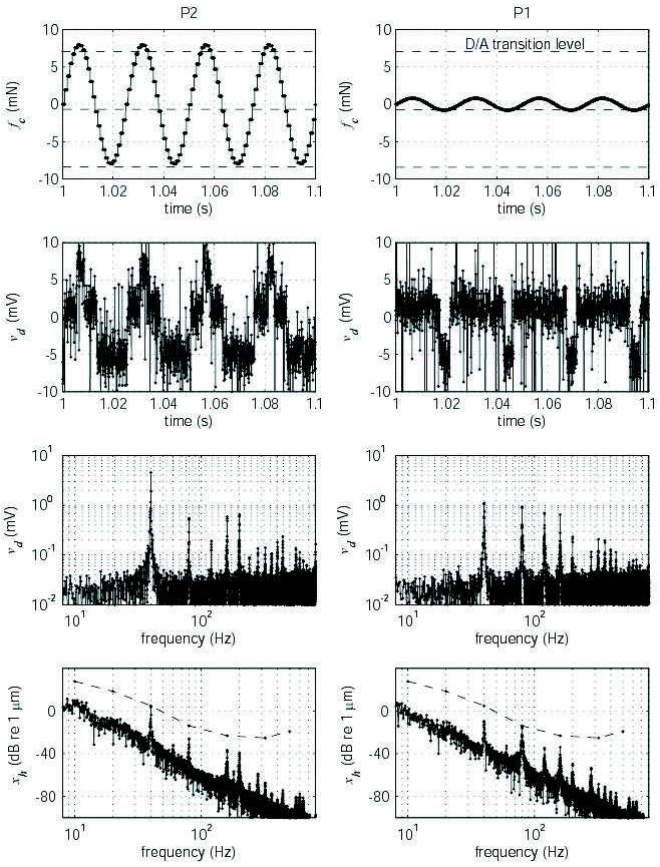

Figure 6: Data from Premium for P2 and P1 at 40 Hz threshold levels.

mium at 40 Hz are near the resolution value of the D/A converter. This coarse quantization by the D/A created significant harmonic distortion. Many of the harmonics observed in the spectral plot of V_d are also present in the displacement spectral data (x_h) for P2 as shown in the figure. Despite a resolution on f_c of 8 mN, the commanded force threshold (A_c)for P1, P4 and P5 with the Premium at 40 Hz are an order of magnitude less than the D/A resolution. Inspection of the temporal and spectral data shown for P1 in Fig. 6 explains this phenomenon. Because the low amplitude f_c signal crosses a D/A transition, albeit slightly, there is a jump from 0 mV to -5 mV on V_d. Furthermore, because f_c is not centered on the D/A transition, the D/A signal has a duty cycle of around 25%. This is evident in the spectral plot of V_d by the lower 40 Hz component and higher 80 Hz component than the spectral data collected from P2. Furthermore, the spectral data for x_h shows the 40 Hz component is subthreshold while the 80 Hz component is at the threshold levels identified by Israr et al. Consequently, those participants that detected lower A_c at 40 Hz were instead detecting the 80 Hz harmonic. Further reduction in the amplitude of f_c would prevent the signal from crossing the transition value of -0.7 mN all together and results in an amplitude of x_h of zero. For this reason, participants described a very noticeable distinction between the signals at levels they could detect and at levels they could not. This was particularly true at 160 Hz. All participants could perceive the lowest non-zero signal afforded by the D/A.

5.2 Amplifier Nonlinearities

Investigation into the internal signals of the amplifier of the Premium showed that the amplifier exhibits offset, drift, hysteresis, and delay. While we don't quantify each of these phenomenon here, we will show their combined effects on x_h. To isolate the distortion created by the amplifiers, we first sent a commanded force signal at 40 Hz and an amplitude near the threshold value, but with a D/A resolution of 20 times the stock Premium D/A resolution. These data are shown in column (a) of Fig. 7. We then bypassed the amplifier and directly commanded voltage to the Premium motors with the NI DAQ board. Again, the 5 mA drive capability of the NI boards was sufficient to drive the Premium directly for this experiment. These data are shown in column (b) of Fig. 7 for comparison. Any discrepancies in $\ddot{x}_h$ and x_h between the two data sets can be attributed exclusively to the amplifier. We note that there is a significant difference between the data. The harmonic distortion created by the Premium amplifiers is supra-threshold.

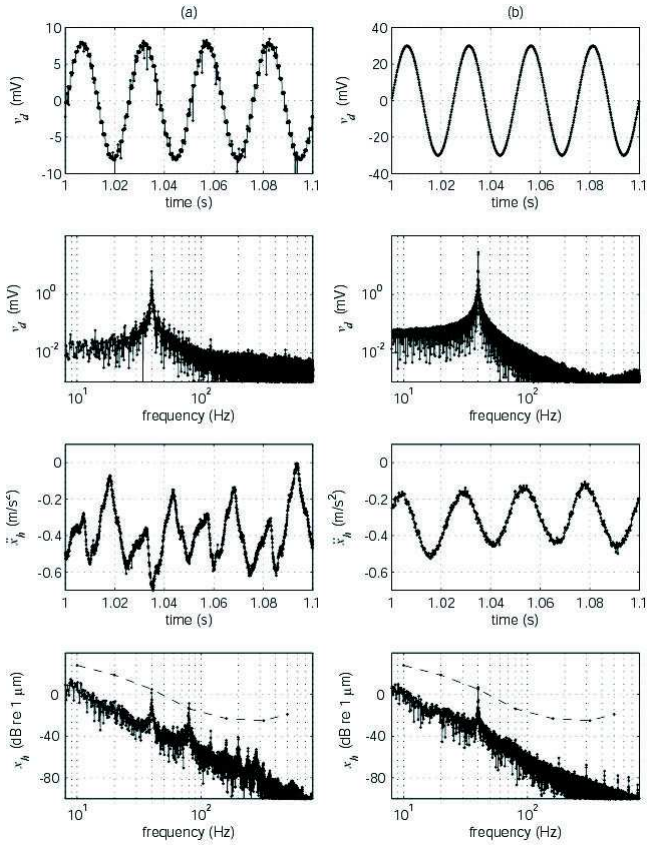

Figure 7: Amplifier distortion data: (a) data sent through Premium amplifiers, (b) data sent through high fidelity amplifiers.

The amplifiers in the Premium we used are 300 series Copley Amplifiers (Copley Controls Corp, Canton, MA). These amplifiers use a drive-brake PWM scheme to modulate current output. This PWM scheme modifies the duty cycle on a square wave whose rails are at 0 V and 30 V in the forward direction. In order to reverse the current direction, there is a switch that enables the PWM rails to change to 30 V and 0 V respectively. This transition has hysteresis, drift, and time delay. This behavior contributes to harmonics observed in the accelerometer data. In contrast, both the Falcon and Omni operate on a locked anti-phase scheme in which the rails are at $\pm$30 V and $\pm$18 V respectively. Consequently, this behavior is not exhibited by these devices.

5.3 Stiction

Inspection of the accelerometer data for both the Falcon and the Omni show stiction plays a dominant role in both threshold levels and the presence of harmonics. To quantify the stiction and its effect on the presentation of sinusoidal signals, we sent each device a 40 Hz signal (f_c) whose amplitude ramped up and then down as a linear function of time. We repeated the test with a 160 Hz signal. The accelerometer was measured while P1 held the stylus. Fig. 8 shows the results of the 40 Hz test on the Falcon and Omni.

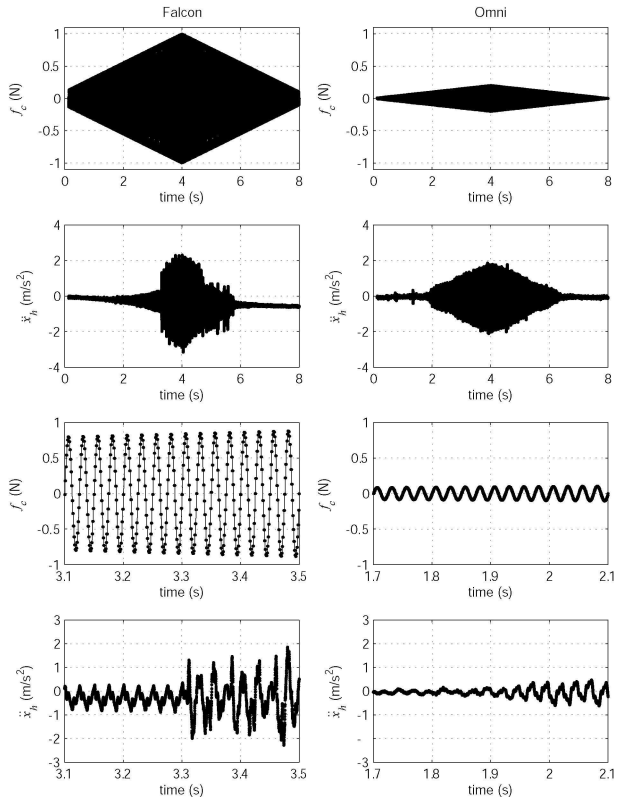

Figure 8: Ramp up and down amplitude on 40 Hz commanded force - bottom two plots show a smaller time window of the same data shown in the top two plots.

From the figure, we can deduce that the stiction is broken on the ramp up when the amplitude of f_c exceeds 0.84 N (0.48 N at 160 Hz). On the ramp down, the amplitude at which the stiction fully re-engages is 0.61 N (0.31 N at 160 Hz). For the Omni the stiction is broken at 0.099 N and 0.12 N on the ramp up for 40 Hz and 160 Hz respectively and 0.079 N and 0.10 N on the ramp down. These f_c values are consistent with the threshold A values obtained with the Falcon and Omni. The lower two plots for the Falcon and Omni of Fig. 8 show a more narrow time window centered about the break-point for stiction. Notice that even when the reference amplitude is high enough to break the stiction, the stiction still re-engages at every peak and valley of the force/acceleration profile. In these instances the velocity is zero and the stiction can re-engage. The disengagement and re-engagement of stiction, coupled with the device linear dynamics, is the primary source of the harmonics observed on both the Falcon and the Omni. The sporadic response seen in the time domain is caused by the device disengaging and reengaging the stiction over time. Participant-induced motion was observed to occasionally break the stiction, thereby reducing the amplitude of f_c to break the stiction.

6 Conclusion

In this paper, we investigated the ability of three commercially available haptic devices to render temporal sinusoids as measured by a psychophysical displacement detection experiment. We compared the performance of these haptic devices to that of a linear voice-coil actuator used as a "gold standard". We found that of the Premium, Omni, and Falcon, none were capable of rendering perceptually distortion-free, periodically regular vibrations at detection threshold levels. Low D/A converter resolution and poor amplifier linearity caused significant harmonic distortion in the Premium. Harmonics, rather than the reference frequency, were shown to be the source of detection. Detection thresholds on the Omni and Falcon could not be achieved because motions at these levels were prevented by device static friction. Device cost was clearly no indicator of the ability of a device to perform sufficiently well for these experiments as none of the devices performed adequately.

An implication of our findings is that the Premium could render perceptually distortion-free, periodically regular vibrations if its D/A resolution and amplifier linearity were improved. Furthermore, the Falcon and Omni would perform equally well in these experiments if their static friction were reduced. Our future work will attempt to either modify or mask these attributes to validate this implication. Furthermore, we will develop psychophysically-based design guidelines for these attributes.

Acknowledgements

This work was supported in part by Sandia National Laboratories.

References

[1] P. Mouroulis. Contrast sensitivity in the assessment of visual instruments. *Assessment of Imaging Systems: Visible and Infrared SPIE*, 274:202–210, 1981.

[2] T.A. Kern, A. Schaeffer, and R. Werthschutzky. An interaction model for the quantification of haptic impressions. *EuroHaptics*, pages 139–145, 2008.

[3] S. Choi and H.Z. Tan. Perceived instability of virtual haptic texture. i. experimental studies. *Presence*, 13(4):395–415, 2004.

[4] S. Choi and H.Z. Tan. Perceived instability of virtual haptic texture. ii. effect of collision-detection algorithm. *Presence*, 14(4):463–481, 2005.

[5] S. Choi and H.Z. Tan. Perceived instability of virtual haptic texture. iii. effect of update rate. *Presence*, 16(3):56–60, 2007.

[6] G. Campion and V. Hayward. Fundamental limits in the rendering of virtual haptic interfaces. In *WHC 05*, pages 263–270, 2005.

[7] S.J. Lederman, R.L. Klatzky, C.L. Hamilton, and G.I. Ramsay. Perceiving roughness via a rigid probe: Psychophysical effects of exploration speed and mode of touch. *Haptics-e (http://www.haptics-e.org)*, 1999.

[8] S.J. Bolanowski, G.A. Gescheider, R.T. Verrillo, and C.M. Checkosky. Four channels mediate the mechanical aspects of touch. *Journal of the Acoustic Society of America*, 84(5):1680–1694, 1988.

[9] R. Johansson and A. B. Vallbo. Tactile sensory coding inthe glabrous skin of the human hand. *Trends in Neuroscience*, 6:27–31, 1983.

[10] http://www.chai3d.com.

[11] H. Levitt. Transformed up-down methods in psuchoacoustics. *The Journal of the Acoustical Society of America*, 49:467–477, 1971.

[12] A. Israr, S. Choi, and H.Z. Tan. Detection threshold and mechanical impedance of the hand in a pen-hold posture. In *Proceedings of the 2006 IEEE/RSJ International Conference on Intelligent Robotics and Systems*, pages 472–477, Beijing, China, 2006.

[13] V. Hayward and O.R. Astley. Performance measures for haptic interfaces. In *Proceedings of Robotics Research: The 7th International Symposium*, pages 195–207, 1996.